Atmos. Meas. Tech. Discuss., 8, 8859–8902, 2015
www.atmos-meas-tech-discuss.net/8/8859/2015/
doi:10.5194/amtd-8-8859-2015

Atmospheric Measurement Techniques Discussions

The development and evaluation of airborne in situ N_2O and CH_4 sampling using a Quantum Cascade Laser Absorption Spectrometer (QCLAS)

J. R. Pitt[1], M. Le Breton[1], G. Allen[1], C. J. Percival[1], M. W. Gallagher[1], S. J.-B. Bauguitte[2], S. J. O'Shea[1], J. B. A. Muller[1], M. S. Zahniser[3], J. Pyle[4], and P. I. Palmer[5]

[1]School of Earth, Atmospheric and Environmental Sciences, University of Manchester, Oxford Road, Manchester, M13 9PL, UK
[2]Facility for Airborne Atmospheric Measurements (FAAM), Building 125, Cranfield University, Cranfield, Bedford, MK43 0AL, UK
[3]Aerodyne Research, Inc., Center for Atmospheric and Environmental Chemistry, Billerica, Massachusetts, USA
[4]Centre for Atmospheric Science, University of Cambridge, Cambridge CB2 1EW, UK
[5]School of GeoSciences, The University of Edinburgh, Edinburgh, EH9 3JN, UK

Received: 30 June 2015 – Accepted: 28 July 2015 – Published: 27 August 2015

Correspondence to: J. R. Pitt (joseph.pitt@manchester.ac.uk)

Published by Copernicus Publications on behalf of the European Geosciences Union.

AMTD
8, 8859–8902, 2015

Abstract

Spectroscopic measurements of atmospheric N_2O and CH_4 mole fractions were made on board the FAAM (Facility for Airborne Atmospheric Measurements) large Atmospheric Research Aircraft. We present details of the mid-IR Aerodyne Research Inc. Quantum Cascade Laser Absorption Spectrometer (QCLAS) employed, including its configuration for airborne sampling, and evaluate its performance over 17 flights conducted during summer 2014. Two different methods of correcting for the influence of water vapour on the spectroscopic retrievals are compared and evaluated. A new in-flight calibration procedure to account for the observed sensitivity of the instrument to ambient pressure changes is described, and its impact on instrument performance is assessed. Test flight data linking this sensitivity to changes in cabin pressure is presented. Total 1σ uncertainties of 1.81 ppb for CH_4 and 0.35 ppb for N_2O are derived. We report a mean difference in 1 Hz CH_4 mole fraction of 2.05 ppb (1σ = 5.85 ppb) between in-flight measurements made using the QCLAS and simultaneous measurements using a previously characterised Los Gatos Research Fast Greenhouse Gas Analyser (FGGA). Finally, a potential case study for the estimation of a regional N_2O flux using a mass balance technique is identified, and the method for calculating such an estimate is outlined.

1 Introduction

CH_4 and N_2O emissions together comprise 38 % of the total global radiative forcing attributable to emissions of well-mixed greenhouse gases (Myhre et al., 2013). N_2O is also a major component of stratospheric chemical cycles, acting as the largest contributing species towards stratospheric ozone depletion, and predicted to remain so throughout the 21st century (Ravishankara et al., 2007). CH_4 emissions can also lead to the formation of tropospheric ozone through reaction with OH radicals, leading to

AMTD
8, 8859–8902, 2015

air quality issues associated with potentially dangerous respiratory problems in many cities across the world (Ebi and McGregor, 2008).

The globally averaged atmospheric abundances of CH_4 and N_2O have increased respectively from 722 ± 25 ppb to 1803 ± 2 ppb and 270 ± 7 ppb to 324.2 ± 0.2 ppb in the period 1750–2011 (Hartmann et al., 2013). However, the relative contribution of individual sources and sinks to the atmospheric abundance of both species is highly uncertain (Ciais et al., 2013; Kirschke et al., 2013). Top-down, measurement based approaches can provide important constraints on these global budgets, both through direct estimation of sectorally and/or regionally disaggregated emissions using atmospheric inversion models (Fraser et al., 2013; Thompson et al., 2014), and by enabling validation of the process models used to compile bottom-up emission inventories (Krinner et al., 2005; O'Shea et al., 2014b). Representative sampling on regional and national scales can also act as an important aid to establishing effective emission reduction policies at both national and international levels.

In situ aircraft-based measurements form an important part of this top-down approach, enabling high-resolution sampling on regional scales (e.g. O'Shea et al., 2013a), vertical profile measurement (e.g. Wofsy et al., 2011), and sampling in remote regions far from ground stations (e.g. Kort et al., 2012). Greenhouse gas flux estimates can then be made using mass balance (Karion et al., 2013; O'Shea et al., 2014a; Peischl et al., 2015), eddy covariance (Ritter et al., 1992; Hiller et al., 2014; Yuan et al., 2015) or inverse modelling techniques (Kort et al., 2008; Polson et al., 2011; Xiang et al., 2013), the latter frequently in association with ground-based measurements (Miller et al., 2013). Aircraft measurements can also be used to validate both ground-based and satellite-based remote sensing techniques, forming an important link across a wide range of spatial and temporal measurement scales (Tanaka et al., 2012; Wecht et al., 2012).

During summer 2014, the FAAM (Facility for Airborne Atmospheric Measurements) large Atmospheric Research Aircraft (hereafter referred to as the FAAM aircraft) participated in the GAUGE (Greenhouse gAs UK and Global Emissions) and MAMM

AMTD
8, 8859–8902, 2015

(Methane and other greenhouse gases in the Arctic: Measurements, process studies and Modelling) measurement campaigns. This aircraft component of the GAUGE campaign focussed on greenhouse gas measurement around the UK, to allow emission estimates to be made in conjunction with both inverse modelling and mass balance techniques. An important element of this campaign was to better constrain emissions from the agricultural sector, which is the second largest contributor (after the energy sector) towards the UK's total greenhouse gas emissions, producing N_2O through the use of nitrogen-based fertilisers and CH_4 by enteric fermentation in livestock (Webb et al., 2014). The MAMM campaign focussed on improving understanding of Arctic CH_4 emissions, dominated by biogenic emission from natural wetlands (Zhuang et al., 2006), in order to help better constrain measurement-derived global CH_4 budgets and to allow comparison against the emissions predicted by regional land surface models (O'Shea et al., 2014b). Accurate measurement of CH_4 and N_2O on board the FAAM aircraft was therefore of critical importance during these campaigns.

Infrared (IR) spectroscopy is frequently employed for airborne measurement of greenhouse gas mole fractions (Chen et al., 2010; O'Shea et al., 2013b; Santoni et al., 2014), enabling high frequency measurement (usually ≥ 1 Hz) and small instrument response times (of the order seconds). Many instruments make use of the superior lasers, optics and detectors available at near-IR wavenumbers of $\sim 6000\,cm^{-1}$ (Baer et al., 2002; Crosson, 2008). However, line strengths for CH_4 and N_2O are of the order 100 and 100 000 times stronger respectively in the mid-IR spectral region of ~ 1000–$4000\,cm^{-1}$ (Rothman et al., 2013). For CH_4 these competing effects lead instruments operating in both spectral ranges to achieve broadly comparable performances. For N_2O, however, the comparatively weak line strengths in the near-IR, coupled with the lower atmospheric abundance of N_2O, make mid-IR spectroscopy much more suitable for atmospheric measurement. Rannik et al. (2015) find that the best long-term and short-term precisions for N_2O measurement are obtained using continuous-wave quantum cascade laser (QCL) based instruments, which operate in the mid-IR region.

AMTD
8, 8859–8902, 2015

In this paper we discuss the development of an airborne measurement system for CH_4 and N_2O, using a mid-IR, continuous-wave, Aerodyne Research Inc. Quantum Cascade Laser Absorption Spectrometer (QCLAS) on board the FAAM aircraft. We focus on measurements from the GAUGE and MAMM campaigns conducted during summer 2014.

Details of the direct absorption spectroscopy and associated spectral retrieval algorithm employed are given in Sect. 2, including the empirically derived correction for the presence of water vapour. The configuration and optimisation of the sample and calibration air flow systems for airborne measurement are also presented in this section. In Sect. 3, calibration procedures used to tie the data to the WMO (World Meteorological Organization) greenhouse gas scale are described and assessed, both through analysis of in-flight calibration data and comparison with simultaneous CH_4 measurements using a Los Gatos Research Fast Greenhouse Gas Analyser (FGGA, Model RMT-200; described by O'Shea et al., 2013b). Section 4 presents N_2O data from GAUGE flight B868 in more detail, and outlines how this data could be used in combination with a mass balance technique to estimate a regional N_2O flux for the northwest of England. Finally, the key findings of this work are summarised in Sect. 5.

2 Operational design

2.1 Instrument specification

In this section we briefly describe the operating principles of the Aerodyne Research Inc. Quantum Cascade Laser Mini Monitor used to measure N_2O and CH_4 on board the FAAM aircraft. This instrument uses a mid-IR, thermoelectrically cooled, continuous-wave, distributed feedback QCL (Alpes Laser, Switzerland) as a light source. The laser beam is directed through an astigmatic Herriott multipass absorption cell, providing an effective optical pathlength through the sample of 76 m (McManus et al., 1995), and collected by a thermoelectrically cooled photovoltaic detector (Vigo Systems, Poland).

AMTD
8, 8859–8902, 2015

The output frequency of the QCL is scanned over a small spectral region (1275.3–1275.8 cm^{-1}), containing ro-vibrational N_2O, CH_4 and H_2O line transitions, by repeatedly ramping the laser current whilst holding the laser at a constant temperature. The laser is swept across this region at a rate of ~ 5 kHz, with a measurement of the detector's zero-light output (noise-equivalent-signal) recorded at the end of each sweep by dropping the current below the laser threshold (such that there is no emission from the laser). Because the linear current ramp does not produce a precisely linear frequency response from the laser, it is necessary to determine the tuning rate using a Germanium etalon, which can be placed in the path of the beam before the multipass cell.

The laser temperature is held at ~ −23 °C using a Peltier cooler. Excess heat is removed using a coolant fluid, which is recirculated and maintained at ~ 25 °C by a CustomChill thermoelectric liquid chiller (CRAL300DHP-12; CustomChill, USA). The optical layout of the instrument is described in detail by Nelson et al. (2004), although our use here of a continuous-wave laser rather than a pulsed laser allows for removal of the beamsplitter and the incorporation of two additional mirrors to aid the adjustment of beam alignment prior to entering the cell.

2.2 TDLWintel software

The laser current control and mole fraction retrievals were performed using the TDLWintel software package, details of which are provided by Nelson et al. (2002). In brief, this retrieval relies on the Beer–Lambert law, given by;

$$\frac{I(\nu)}{I_0(\nu)} = \exp\left(-\alpha(\nu,P,T)\,nCL\right), \quad (1)$$

where L is the path length of the beam through the absorber, C is the concentration of sample gas, n is the absorber mole fraction and $\alpha(\nu,P,T)$ is the frequency, pressure and temperature dependent absorption cross section of the absorber. The intensity $I(\nu)$ is measured by the detector, which also measures the background intensity $I_0(\nu)$ at window wavelengths outside the wings of target absorption lines. A polynomial fit is

AMTD
8, 8859–8902, 2015

applied to the data obtained at these non-absorbing wavelengths such that variation in baseline intensity measurement, due to changes in both laser output and detector sensitivity across the measured spectral range, can be subtracted from the spectrum (Zahniser et al., 1995).

In order to determine the mole fraction of a target species at a sampling rate of 1 Hz, TDLWintel fits a Voigt line shape profile to an averaged spectrum, consisting of ~ 5000 individual laser sweeps, using a Levenberg–Marquardt retrieval algorithm. Line strengths and positions are taken from the HITRAN 2012 database (Rothman et al., 2013). The pressure and temperature of the sample are continuously measured by in situ sensors positioned within the sample gas flow on the outlet of the cell, allowing air broadening effects to be considered in the retrieval.

2.3 Configuration for airborne measurement

The QCLAS is mounted on a rack inside the cabin of the FAAM aircraft, with a rearward facing, 3/8″ outer diameter, stainless steel inlet inserted through a customised window blank (Avalon Aero Ltd., UK). The sample flow line consists of Swagelok 1/4″ outer diameter PFA Teflon tubing, partly encased within the inlet, and forming a pressure seal via a bored-through Swagelok 3/8″ to 1/4″ reducing union. Figure 1 shows a schematic of the QCLAS air sampling system including the configuration for delivering calibration gas to the sample cell. The sample flow line is ~ 2.5 m in length from the inlet tip to the pressure controller. Sample flow rate is measured using a 30 SLPM (Standard Litres Per Minute) mass flow meter (M10MB01334CS3BV, MKS Instruments UK Ltd, UK), placed directly upstream of a 0.5 µm sintered particle filter (SS-4F-05, Swagelok, USA).

The choice of sample cell pressure is a balance between two effects: higher pressures increase the absorption, thus improving the signal-to-noise ratio of the measurement, whilst pressure broadening of the spectral lines increases spectral overlap and line mixing (as discussed by Zahniser et al., 1995). Airborne operation is also compli-

AMTD
8, 8859–8902, 2015

cated by the large variation in inlet pressures typically encountered over the course of a flight (down to ~ 250 hPa at 10 km altitude).

Control of the cell pressure is provided by an electronic pressure controller (640A-13TS1V62V, MKS Instruments UK Ltd, UK) placed upstream of the sample cell, as shown in Fig. 1. This maintains a constant pressure by automatically adjusting an internal valve to restrict the flow of air through it. As the inlet pressure decreases, the valve is set to a progressively more open position. The minimum inlet pressure that can be sampled whilst maintaining any given cell pressure is attained when the pressure controller valve reaches its fully open position. This minimum inlet pressure is then equal to the sum of the (chosen) cell pressure and the pressure drops across each component of the inlet system (including the fully open pressure controller valve). Hence choosing a lower cell pressure decreases this minimum inlet pressure, enabling the cell to be held at constant pressure up to a higher altitude. A cell pressure of 68.9 ± 3.6 hPa (at 1σ) was used during the GAUGE and MAMM campaigns.

Air is pulled through the system using a single stage scroll pump (Edwards XDS10, Edwards, UK). A throttle valve (253B-1-40-1, MKS Instruments UK Ltd, UK) positioned between the sample cell outlet and the pump inlet is used to control the flow rate through the system. This again is a balance between the desire to decrease the instrument response time, favouring a faster flow rate, and the desire to reduce the total pressure drop between the inlet and the sample cell, favouring a slower flow rate. Throughout the GAUGE and MAMM campaigns the valve was set to 18 % of its fully open position, resulting in a constant mass flow rate of 1.43 ± 0.21 SLPM (at 1σ) down to inlet pressures of ~ 380 hPa. At lower inlet pressures both the mass flow rate and the cell pressure were reduced.

Laboratory tests were performed to establish the effect of cell pressure changes on the mole fractions retrieved when sampling a compressed air cylinder. The variability in retrieved mole fraction was found to be no greater across cell pressures typically encountered during high altitude flying (inlet pressures below 380 hPa; cell pressures down to ~ 46 hPa) than across the range experienced during low altitude flying (inlet

AMTD
8, 8859–8902, 2015

pressures above 380 hPa; cell pressures between 65 and 76 hPa). It was therefore deemed unnecessary to filter data according to the absolute cell pressure value. However, rapid changes in pressure were found to impact upon the retrieved mole fractions; consequently data was removed whenever the 10 s standard deviation in cell pressure exceeded 0.1 Torr (13.3 Pa).

The response time of the system was determined in the laboratory (at 1017 hPa inlet pressure) by overflowing the inlet with N_2 from a compressed gas cylinder. The e-folding time of the system was determined using an exponential fit to the decay in retrieved mole fractions, and was found to be 0.68 ± 0.12 s (mean $\pm 1\sigma$). The inlet lag time was given by the time between turning on the N_2 flow and the first drop in retrieved mole fractions. In this laboratory test it was found to be in the range 2–3 s; however, we expect this lag time to decrease with altitude (up to ~ 380 hPa) as the volumetric flow rate of the system scales inversely with air density (for a constant mass flow rate).

In principle the Beer–Lambert relationship described above can be used to retrieve absolute mole fractions. However, in-flight calibration is commonly used to account for instrumental drift when using optical-based measurements (e.g. O'Shea et al., 2013b; Santoni et al., 2014), as external variables such as temperature and pressure can undergo significant variation during a flight. Our system employs three calibration standards to scale the data and assess instrument performance, as described in Sect. 3.1.

The 3 calibration standards are stored in 10 L carbon fibre hoop-wrap cylinders (BFC 124-136-002, Aluminium Alloy 7060, Luxfer, UK), which are filled to ~ 300 bar and mounted to the QCLAS rack. Each cylinder is fitted with a high pressure brass valve (C215, Rotarex, Luxembourg), screwed into the cylinder collar using PTFE (polytetrafluoroethylene) tape. An all brass adapter connects this to instrument-grade stainless steel tubing of 1/8″ outer diameter, specially cleaned for high purity service (21512, Thames–Restek, UK). This tube joins each cylinder to a separate single-stage diaphragm brass regulator (44-2212-244-1382, TESCOM, UK). On the low pressure side of the regulator Swagelok 1/8″ outer diameter PFA Teflon tubing is used. Three 3-way valves (009-0294-900, Parker–Hannifin, USA) and one 2-way valve (009-0089-

AMTD
8, 8859–8902, 2015

900, Parker–Hannifin, USA) are used to select the flow from the desired calibration cylinder (a fourth port allows sampling from an external cylinder). The flow rate is set using a mass flow controller (1179A01314CS1BV, MKS Instruments UK Ltd, UK) to provide an overflow of calibrant at the inlet (upstream of the mass flow meter).

2.4 Water vapour correction

The influence of water vapour on spectral retrievals can be very significant (e.g. Allen et al., 2014), particularly given the wide range of natural water vapour concentrations typically encountered over the course of a flight (from a small fraction of a percent to many percent in the troposphere alone). To ensure comparability between measurements made at different humidity levels it is necessary to remove this effect and report dry mole fractions.

Many opt to circumvent the need to correct for this influence by drying the sample air before it enters the instrument, often using a combination of Nafion gas dryers and dry ice traps (e.g. Daube et al., 2002; Peischl et al., 2010; Santoni et al., 2014). The advantage of this approach is obvious, as any empirically derived correction for the influence of water vapour will contribute, often significantly, to the overall uncertainty of the measurements. However, there are several disadvantages associated with drying the sample, as discussed in detail by Rella et al. (2013). Of particular relevance for the QCLAS system described here are the issues associated with increasing the pressure drop across the inlet system, increasing the residence time in the inlet system, and the logistical problems of supplying dry ice to remote field locations and transporting it in a sealed cabin environment.

In cases such as this, where the sample is not dried, an empirical correction must be derived in order to account for the water vapour influence. Typically this involves applying a scale factor to the retrieved mole fractions, with its form and coefficients determined through laboratory experiment. Rella et al. (2013), O'Shea et al. (2013b) and Zellweger et al. (2012) employ this approach across a variety of spectroscopic instruments. However, a recently added feature of the TDLWintel software allows the

AMTD
8, 8859–8902, 2015

effect of line broadening (in addition to sample dilution) due to the presence of water vapour to be included in the spectroscopic retrieval itself. Instrument-specific ratios quantifying the broadening due to water vapour in terms of the broadening due to air must be derived empirically for each species. Water corrected mole fractions are then determined by first retrieving the water vapour mole fraction, then combining this result with the appropriate water broadening coefficients in the retrieval of the other species.

Here we compare the effectiveness of these two approaches in the case of the QCLAS. As TDLWintel retains the measured raw spectral data, it was possible to do this by reanalysing the same dataset, varying only the way in which the water vapour influence was treated in the retrieval. The data here was gathered in four separate laboratory experiments, each using an identical experimental setup to that employed by O'Shea et al. (2013b), who provide a full description. In summary, dry compressed air was humidified to a variety of different water vapour mole fractions, spanning the range of 0–2 % typically measured in flight. Between each measurement of humid air, a dry reference was sampled, using a dry ice trap to reduce the sample dew point to less than −60 °C. It should be noted that by re-drying the air downstream of the humidifier we accounted for any dissolution of gases in the humidifier, and the temperature dependence of this effect.

The first approach used the following relationship to scale the measurements of the wet sample to corresponding dry mole fractions:

$$X_{\mathrm{dry}} = \frac{X_{\mathrm{wet}}}{a + b\mathrm{H_2O}}, \tag{2}$$

where X_{wet} and X_{dry} are the raw and the scaled, water corrected mole fractions respectively for species X, and $\mathrm{H_2O}$ represents the retrieved mole fraction of water vapour. Coefficients a and b were derived by performing a weighted least orthogonal distance regression of $X_{\mathrm{wet}}/X_{\mathrm{dry}}$ as a function of $\mathrm{H_2O}$ for data from all four experiments.

The empirical values for the QCLAS were found to be $a = 1.00096$, $b = -0.0154563\,\%^{-1}$ for N_2O, and $a = 1.00071$, $b = -0.0136929\,\%^{-1}$ for CH_4. The uncer-

AMTD
8, 8859–8902, 2015

tainties associated with these values can be quantified by the residuals of this regression for CH_4 and N_2O, shown in Fig. 2. The RMS (root mean square) values for these residuals are 2.5 and 0.50 ppb for CH_4 and N_2O respectively.

It is apparent from Fig. 2 that substantially different behaviour was observed on 20 June 2014 when compared to the three other experiments. This is likely to be associated with a lack of long-term stability in the retrieval of H_2O mole fraction, largely driven by variability in baseline intensity in the region of the H_2O absorption line. The effect of this baseline instability can be reduced by using the spectroscopic water vapour correction method described below.

The second, spectroscopic, water vapour correction method used the water broadening function in TDLWintel to correct for the influence of water vapour. Reanalyses of the raw spectra were performed using a variety of different water broadening coefficients in the retrieval. For each coefficient, the difference between the retrieved wet mole fraction and the corresponding dry measurement was calculated at every water vapour level used during the four experiments. The RMS difference for each coefficient, averaged over the entire dataset, is shown in Fig. 3. It can be seen that the correction performed best using water broadening coefficients of 1.6 and 1.8 for CH_4 and N_2O respectively. These optimal coefficients resulted in RMS differences between corresponding wet and dry measurements of 1.6 ppb for CH_4 and 0.32 ppb for N_2O; these are the values used to determine the contribution of uncertainty in this water vapour correction to the total measurement uncertainty of the instrument.

It was thus concluded that in this case a better correction for the influence of water vapour was obtained using the spectroscopic correction performed by the TDLWintel software than was achieved by scaling the wet mole fractions according to Eq. (2). All flight data presented in this paper has been reanalysed using this spectroscopic correction, with empirically derived water broadening coefficients of 1.6 and 1.8 for CH_4 and N_2O respectively.

AMTD
8, 8859–8902, 2015

3 Data quality

Systematic instrumental error associated with changes in external variables such as temperature and pressure can be compensated for by repeated sampling of calibration gas. During airborne sampling an instrument is exposed to rapid changes in these variables over a wide range of values, hence regular calibration is required.

In this section we first describe the calibration procedure used during the two campaigns, and explain the rationale behind it. We then seek to diagnose and understand the sources of systematic error which remain uncaptured by this calibration. Finally, we describe an alternative calibration procedure designed to better address these key sources of error, and evaluate the effect of both methods on the overall data quality.

3.1 Original calibration procedure

The in-flight calibration procedure employed throughout the GAUGE and MAMM campaigns was in principle similar to that described by O'Shea et al. (2013b). The data was scaled using two cylinders of known composition, traceable to the WMO greenhouse gas scale (WMO, 2009), whose mole fractions spanned the normal measurement range for N_2O and CH_4. By sequentially pumping gas from these cylinders through the system and comparing the retrieved mole fractions to their WMO-traceable values, two reference points could be established for the QCLAS on the WMO scale. By assuming a linear relationship, the "true" mole fraction corresponding to each retrieved QCLAS mole fraction was given by interpolating the scale between the two reference points. For each calibration a scale factor (M_x) and zero-offset (C_x) were found using:

$$M_x = \frac{\left(X_{\text{high, WMO}} - X_{\text{low, WMO}}\right)}{\left(X_{\text{high, meas}} - X_{\text{low, meas}}\right)}, \quad (3)$$

$$C_x = X_{\text{high, WMO}} - M_x \cdot X_{\text{high, meas}}, \quad (4)$$

AMTD
8, 8859–8902, 2015

where $X_{\text{high, WMO}}$ and $X_{\text{low, WMO}}$ are the "true" WMO-traceable mole fraction values, and $X_{\text{high, meas}}$ and $X_{\text{low, meas}}$ are the measured mole fraction values, for the high and low calibration cylinders respectively, for a given species X.

These two cylinders were sampled sequentially on an approximately hourly basis and the values for M_x and C_x were linearly interpolated between calibrations. The raw data was then calibrated by applying:

$$X_{\text{cal}}(t) = M_x(t) \cdot X_{\text{raw}}(t) + C_x(t). \quad (5)$$

In order to check that both interpolation between the two cylinder mole fraction values and temporal interpolation between hourly calibrations were justified, a third WMO-traceable "target" cylinder containing intermediate CH_4 and N_2O mole fractions was measured approximately mid-way between the hourly high-low span calibrations. Applying the above calibration to this target cylinder measurement and comparing the resulting calibrated mole fractions with the WMO-traceable values for the cylinder enabled errors associated with this method to be quantified. Raw CH_4 data demonstrating a typical calibration cycle is shown in Fig. 4.

This calibration procedure was designed to remove linear drifts acting over timescales of the order of the inter-calibration time, here approximately 1 h. However, analysis of the difference in CH_4 mole fraction between the raw QCLAS data and the calibrated data from the on-board FGGA frequently showed gradients of over 30 ppb in timescales of less than 10 min, as shown for flight B848 in Fig. 5. The FGGA on board the FAAM aircraft has previously been shown not to exhibit any significant systematic errors on this timescale (O'Shea et al., 2013b), suggesting that these gradients represent a source of systematic error in the QCLAS data. Note that although we have compensated here for the lag time between the two instruments using the correlation between the two CH_4 datasets, large deviations from the overall trend with very short durations are present as a result of small differences in the measurement time of large CH_4 enhancements.

AMTD
8, 8859–8902, 2015

Figure 6 shows the same CH_4 data from flight B848 plotted as a function of static pressure, as measured by the aircraft's RVSM (Reduced Vertical Separation Minimum) system. It can be seen that a broadly repeatable pattern exists as a function of pressure, which was found to dominate variability in the raw QCLAS CH_4 data offset with respect to the FGGA over the course of the flight. The same pattern is also exhibited by the offset of the calibration cylinder measurements from the nominal values of the cylinders (also shown), although the absolute value of this offset clearly differs between the cylinders. Similar patterns were observed for the cylinder measurements of N_2O, and across other flights during the two campaigns.

The fact that this variation with pressure can be observed in both the raw sample data and the measurement of dry calibration air confirms that errors in the water vapour correction cannot be responsible. A leak (ingress) into the system also appears implausible, as one would expect this to have the opposite effect on the high and low cylinder measurements, pulling both towards the mole fractions of CH_4 and N_2O present in the aircraft cabin. Santoni et al. (2014) warn of issues associated with fluctuations in sample cell pressure. However, the offsets in retrieved QCLAS mole fractions observed here were found to exhibit no dependence on either sample cell pressure or sample cell temperature, or the rate of change for these variables (as recorded by the pressure and temperature sensors within the sample flow).

The temperature of the cabin air was also recorded as it entered the outer enclosure of the QCLAS, but this again exhibited no clear correlation with the CH_4 data offset. The pressure inside the cabin, however, was not recorded during these campaigns. Subsequent test flights, described in Sect. 3.2 below, suggest that it was variability in this quantity that caused the large gradients in CH_4 offset described above.

3.2 Influence of cabin pressure

In April 2015 a test flight, B903, was flown to further understanding of the underlying issues behind the large gradients in QCLAS CH_4 data described in Sect. 3.1 above. This time cabin pressure data was available throughout the flight, and three deep profiles

AMTD
8, 8859–8902, 2015

were performed whilst the QCLAS sampled compressed air from a calibration cylinder. The first deep profile occurred at the beginning of the flight, whilst the other two were performed ~ 2.5 h later.

Figure 7 shows the offset in retrieved CH_4 and N_2O mole fractions from the known composition of the cylinder as a function of both cabin pressure and RVSM external static pressure. For external pressures between ~ 800 hPa and ~ 1000 hPa these offsets remain roughly constant; this can be seen to correspond to the range of external pressures over which there is no change in cabin pressure. The fact that, for both CH_4 and N_2O, the raw QCLAS measurement offset does not change when the cabin pressure is constant, even when the external pressure is varying, strongly suggests that cabin pressure variability is the primary cause of the large gradients in this offset observed throughout the GAUGE and MAMM campaigns in summer 2014.

A time series of the retrieved mole fraction offsets for the final two profiles is shown in Fig. 8. The influence of changing cabin pressure on these retrieved mole fractions can be characterised as a small scale oscillation superimposed on a larger scale gradient. This large scale gradient appears to be very consistent across the three profiles (see also Fig. 7), whereas the small scale oscillations are not so repeatable.

The likely pathway through which cabin pressure can influence the retrieved mole fractions is through its effect on baseline intensity in the spectral regions close to the absorption lines. There are two potential components to this: the effect of changing absorption in the open path section of the laser, and the effect of changing pressure on the alignment of the instrument's optical components.

To investigate the effect of varying the open path absorption, a further test flight was conducted whilst flowing dry nitrogen through the laser beam enclosure. A simulation was also performed, where open path CH_4 and N_2O absorption were included in the spectral fit for the range of cabin pressures encountered during flight B903, to assess the impact on the retrieved mole fractions. Both of these tests indicated that varying open path absorption contributed negligibly to the observed gradients in retrieved mole fraction over the range of cabin pressures experienced during these flights. Hence we

AMTD
8, 8859–8902, 2015

conclude that these gradients are more likely attributable to small changes in optical alignment associated with cabin pressure variation.

3.3 Pressure-differentiated calibration procedure

As the short term (of order minutes) instrumental drift with pressure had a greater effect in degrading measurement precision than any longer term (of order hours) drift with time, the data was reanalysed using an alternative calibration procedure, designed to reduce the impact of this issue on the overall accuracy of the calibrated measurements. As there was no cabin pressure data available for the GAUGE and MAMM campaigns in summer 2014, it was necessary to use the external static pressure from the aircraft's RVSM system as a proxy. This approach is justified by the strong correlation between cabin pressure and external pressure, and by the results in Sect. 3.4 below.

In this approach values of $M_x(t)$ and $C_x(t)$ for sections of flight at broadly equivalent pressure levels (defined here as a range of variability less than 15 hPa for a period longer than 2 min) were interpolated between any calibrations conducted at a pressure within 15 hPa of the average pressure during that section. Profile data, along with all data at pressure levels where no calibrations were performed, were flagged as poor quality and removed from the analysis. This pressure-differentiated calibration method has the disadvantages of both reducing the amount of calibrated data for the campaigns by 54 % and potentially inducing errors associated with long term instrumental drift, as data can be separated from the corresponding calibration(s) by up to 5 h. The effect on the overall data quality of using this pressure-differentiated calibration procedure is discussed and compared in Sect. 3.4.

It was also found that large roll angles (~ 20° or over), associated with sharp turns of the aircraft, produced short term deviations in retrieved CH_4 and N_2O mole fractions, evident in both the raw and calibrated data. It is likely that this effect is a consequence of slight alignment changes (similar to Sect 3.2 above) caused by the centrifugal force of the turn (no relationship with cabin pressure variability was found). Whilst this effect was clearly secondary to the pressure-dependent variability described above, producing

AMTD
8, 8859–8902, 2015

CH_4 deviations of less than 5 ppb, it was decided to flag all data associated with roll angles of greater than 10° as reduced quality. All calibrated data (using both methods) discussed here has been filtered according to this flag, removing the reduced quality data associated with high roll angles. The application of this filter reduces the total size of the raw dataset by only 7 %.

3.4 Results and discussion

The performance of the QCLAS can be assessed both by comparing the calibrated target cylinder measurements to their corresponding WMO-traceable values and by comparing the calibrated 1 Hz CH_4 sample data with the corresponding measurements from the on-board FGGA. No other instruments on board the FAAM aircraft measured N_2O during the GAUGE or MAMM campaigns, so a direct comparison of sample N_2O mole fractions cannot be made here. Table 1 summarises these results for both the original calibration method described in Sect. 3.1 and the pressure-differentiated calibration method described in Sect. 3.2.

It can be seen from the table that using the pressure-differentiated calibration method significantly improves the accuracy of the QCLAS, both during target cylinder measurements and sample mode. In particular, the standard deviations in QCLAS-target and QCLAS-FGGA differences are substantially reduced compared to the equivalent values produced using the original calibration method. The WMO recommends compatibility between different analyses within 2 ppb for CH_4 and 0.1 ppb for N_2O (WMO, 2013). The fraction of data within these ranges for both the QCLAS-target and QCLAS-FGGA differences using both methods is shown in Table 2. Here again it can be seen that the pressure-differentiated calibration method produces superior results.

Figure 9 shows the offset between the calibrated 1 Hz QCLAS target cylinder measurements and the known content of the cylinder, as histograms for both CH_4 and N_2O. It can be seen here that the improved standard deviations obtained using the pressure-differentiated calibration method result from the removal of outlying data associated with the pressure effect discussed in the previous section. Also shown are

AMTD
8, 8859–8902, 2015

histograms of the QCLAS-FGGA offset for 1 Hz CH_4 sample data, which provide further evidence of the superior performance of the pressure-differentiated calibration method. The data produced using the original calibration method is clearly far less well represented by a Gaussian fit; this is to be expected in the presence of a systematic effect such as that described in Sect. 3 above. In contrast, the Gaussian shape of the pressure-differentiated data is consistent with a random error distribution for both instruments.

The instrument precision can be quantified using the Allan Variance technique (Werle et al., 1993). Table 3 presents the 1σ Allan Precision (over 1, 10 and 108 s) for CH_4 and N_2O, both in a laboratory environment whilst sampling a compressed air cylinder, and in flight during a period of ambient background sampling. These results are similar to those of Santoni et al. (2014), with in-flight 1 Hz precisions here of 0.52 ppb for CH_4 and 0.11 ppb for N_2O.

Finally, a nominal uncertainty for the data can be calculated using the known uncertainties from the water vapour correction experiment, the calibration of the target cylinder to the WMO scale and the in-flight target measurements. Table 4 contains these values for both CH_4 and N_2O using the pressure-differentiated calibration method. The nominal total uncertainties for CH_4 and N_2O are ±1.81 ppb and ±0.35 ppb respectively.

4 Case study

The GAUGE project aims to provide top-down greenhouse gas emission estimates for the UK, which can be used to validate the bottom-up inventory-based estimates required by UK and international legislation. As part of this approach, it is planned to use aircraft data in combination with mass balance techniques (Karion et al., 2013; O'Shea et al., 2014a; Peischl et al., 2015) to estimate regional greenhouse gas emissions. Such analysis is beyond the scope of this technical study, however we present QCLAS data from a single flight here as an exemplar of typical flight data, providing context with regard to scientific case studies which may use this new airborne dataset.

AMTD
8, 8859–8902, 2015

Flight B868 was designed to incorporate upwind and downwind sampling over northwest England to provide a dataset for a mass balance case study. This region contains several large urban areas (Manchester, Liverpool, Leeds and Sheffield) and also includes several areas of agricultural activity, known to be an important anthropogenic source of N_2O (Syakila and Kroeze, 2011). The flight track, coloured by N_2O mole fraction, is shown in Fig. 10. The wind speed and direction, as measured on board the aircraft and taken as an average over 60 s, are represented by wind barbs according to the standard convention where each full barb represents a wind speed of 10 knots. Selected Lagrangian back trajectories using the HYSPLIT (Hybrid Single-Particle Lagrangian Integrated Trajectory) model (Draxler and Hess, 1998) are also shown (representing around 24 h track across the UK mainland in the figure). These trajectories were initiated using endpoints and trajectory end-times selected along the flight track, and modelled with full vertical dynamics using Global Data Assimilation System 1° resolution data.

It can be seen that the N_2O mole fractions measured in the northwest of the domain were enhanced relative to those in the southeast. A relatively consistent south-easterly wind direction (both measured and seen in the trajectories) suggests that this enhancement may enable the use of a mass balance technique to estimate the N_2O flux from an area between this downwind transect and the corresponding upwind measurements using the techniques described by O'Shea et al. (2014a). This requires suitable investigation of the necessary assumptions, which is beyond the scope of this simple example.

It is also striking that there is a relative contrast in the southwest area of the domain, with N_2O mole fractions around 328 ppb (compared with 330 ppb in the northwest). The potential reasons for this small contrast, in terms of airmass history, may be explained by considering both the trajectories and the wind barbs. The trajectories from the northwest domain show recent transport at low altitude (below 1 km) over Greater Manchester and the North West conurbation, whereas southwest trajectories pass over more rural areas. This appears counterintuitive, as we expect the agricultural sector to

AMTD
8, 8859–8902, 2015

be the primary contributor towards N_2O emissions in this region. However, the wind barbs (which represent real measurements) show that there is a complex divergence in the wind-field in the southwest domain, perhaps indicative of a localised sea-breeze circulation that cannot be expected to have been captured at the resolution of the meteorological data that was used to initialise the HYSPLIT trajectories. This sea-breeze circulation could suggest recirculation of maritime air and hence dilution of any moderately enhanced air arriving on the prevailing wind from the east. The differing localised dynamics and airmass histories of the two domains may explain the observed contrast. Further analysis of this may form the basis of future work and this limited example demonstrates the utility of aircraft data in understanding local and regional airmass characteristics.

5 Conclusions

An Aerodyne Research Inc. QCLAS was used to measure N_2O and CH_4 on board the FAAM aircraft during the GAUGE and MAMM campaigns in summer 2014. A relationship between QCLAS measurement error and cabin pressure was found, and a new calibration procedure was adopted to minimise the impact of this effect on the final data. Using this pressure-differentiated calibration method, total uncertainties of ±1.81 ppb and ±0.35 ppb were obtained for the measurement of CH_4 and N_2O respectively.

The sample air was not dried prior to measurement, so a correction for the influence of water vapour on the retrieved mole fractions was required. The performance of two different water vapour correction methods was compared using data from four separate experiments. It was found that the best results were obtained using the water broadening function in the TDLWintel software, which included the effects of water broadening on the CH_4 and N_2O absorption lines directly in the mole fraction retrieval. Experimentally derived coefficients for the ratio of water vapour broadening to air broadening of 1.6 and 1.8 were found to give the best results for CH_4 and N_2O respectively.

AMTD
8, 8859–8902, 2015

Overall instrument performance is found to be broadly comparable with similar studies (e.g. O'Shea et al., 2013b; Santoni et al., 2014) if the pressure-differentiated calibration procedure is used. However, this has the disadvantage of removing 54 % of the measured sample data, including all data during vertical profiles, which are frequently of scientific interest. A priority for improvement is to prevent the large short term drifts in measurement error that necessitate the removal of this data. One potential solution would be to enclose the instrument within a pressure-sealed container. The feasibility of practically implementing this solution on board the FAAM aircraft is currently being studied.

Acknowledgements. The authors would like to thank everyone at FAAM and the numerous people at Avalon Aero and Directflight who assisted with the logistics of installing the QCLAS on the aircraft. J. R. Pitt is in receipt of a NERC CASE studentship in partnership with FAAM, grant number NE/L501/591/1, supervised by G. Allen. This work was supported by the NERC projects: GAUGE (Greenhouse gAs UK and Global Emissions), grant number NE/K002279/1, and MAMM (Methane and other greenhouse gases in the Arctic: Measurements, process studies and Modelling), grant number NE/I029161/1. We are also grateful to the Norwegian Research Council, who partly funded the 2014 MAMM flights through the MOCA (Methane Emissions from the Arctic OCean to the Atmosphere: Present and Future Climate Effects) project.

References

Allen, G., Illingworth, S. M., O'Shea, S. J., Newman, S., Vance, A., Bauguitte, S. J.-B., Marenco, F., Kent, J., Bower, K., Gallagher, M. W., Muller, J., Percival, C. J., Harlow, C., Lee, J., and Taylor, J. P.: Atmospheric composition and thermodynamic retrievals from the ARIES airborne TIR-FTS system – Part 2: Validation and results from aircraft campaigns, Atmos. Meas. Tech., 7, 4401–4416, doi:10.5194/amt-7-4401-2014, 2014.

Baer, D. S., Paul, J. B., Gupta, M., and O'Keefe, A.: Sensitive absorption measurements in the near-infrared region using off-axis integrated-cavity-output spectroscopy, Appl. Phys. B-Lasers O., 75, 261–265, doi:10.1007/s00340-002-0971-z, 2002.

Chen, H., Winderlich, J., Gerbig, C., Hoefer, A., Rella, C. W., Crosson, E. R., Van Pelt, A. D., Steinbach, J., Kolle, O., Beck, V., Daube, B. C., Gottlieb, E. W., Chow, V. Y., Santoni, G. W.,

AMTD
8, 8859–8902, 2015

and Wofsy, S. C.: High-accuracy continuous airborne measurements of greenhouse gases (CO_2 and CH_4) using the cavity ring-down spectroscopy (CRDS) technique, Atmos. Meas. Tech., 3, 375–386, doi:10.5194/amt-3-375-2010, 2010.

Ciais, P., Sabine, C., Bala, G., Bopp, L., Brovkin, V., Canadell, J., Chhabra, A., DeFries, R., Galloway, J., Heimann, M., Jones, C., Le Quéré, C., Myneni, R. B., Piao, S., and Thornton, P.: Carbon and other biogeochemical cycles, in: Climate Change 2013: The Physical Science Basis. Contribution of Working Group I to the Fifth Assessment Report of the Intergovernmental Panel on Climate Change, edited by: Stocker, T. F., Qin, D., Plattner, G.-K., Tignor, M., Allen, S. K., Boschung, J., Nauels, A., Xia, Y., Bex, V., and Midgley, P. M., Cambridge University Press, Cambridge, UK and New York, NY, USA, 465–570, 2013.

Crosson, E. R.: A cavity ring-down analyzer for measuring atmospheric levels of methane, carbon dioxide, and water vapor, Appl. Phys. B-Lasers O., 92, 403–408, doi:10.1007/s00340-008-3135-y, 2008.

Daube, B. C., Boering, K. A., Andrews, A. E., and Wofsy, S. C.: A high-precision fast-response airborne CO_2 analyzer for in situ sampling from the surface to the middle stratosphere, J. Atmos. Ocean. Tech., 19, 1532–1543, doi:10.1175/1520-0426(2002)019<1532:AHPFRA>2.0.CO;2, 2002.

Draxler, R. R. and Hess, G. D.: An overview of the HYSPLIT_4 modelling system for trajectories, dispersion, and deposition, Aust. Meteorol. Mag., 47, 295–308, 1998.

Ebi, K. L. and McGregor, G.: Climate change, tropospheric ozone and particulate matter, and health impacts, Environ. Health Persp., 116, 1449–1455, doi:10.1289/ehp.11463, 2008.

Fraser, A., Palmer, P. I., Feng, L., Boesch, H., Cogan, A., Parker, R., Dlugokencky, E. J., Fraser, P. J., Krummel, P. B., Langenfelds, R. L., O'Doherty, S., Prinn, R. G., Steele, L. P., van der Schoot, M., and Weiss, R. F.: Estimating regional methane surface fluxes: the relative importance of surface and GOSAT mole fraction measurements, Atmos. Chem. Phys., 13, 5697–5713, doi:10.5194/acp-13-5697-2013, 2013.

Hartmann, D. J., Klein Tank, A. M. G., Rusticucci, M., Alexander, L. V, Brönnimann, S., Charabi, Y. A.-R., Dentener, F. J., Dlugokencky, E. J., Easterling, D. R., Kaplan, A., Soden, B. J., Thorne, P. W., Wild, M., and Zhai, P.: Observations: Atmosphere and Surface, in: Climate Change 2013: The Physical Science Basis. Contribution of Working Group I to the Fifth Assessment Report of the Intergovernmental Panel on Climate Change, edited by: Stocker, T. F., Qin, D., Plattner, G.-K., Tignor, M., Allen, S. K., Boschung, J., Nauels, A.,

AMTD
8, 8859–8902, 2015

Xia, Y., Bex, V., and Midgley, P. M., Cambridge University Press, Cambridge, UK and New York, NY, USA, 159–254, 2013.

Hiller, R. V, Neininger, B., Brunner, D., Gerbig, C., Bretscher, D., Künzle, T., Buchmann, N., and Eugster, W.: Aircraft-based CH_4 flux estimates for validation of emissions from an agriculturally dominated area in Switzerland, J. Geophys. Res.-Atmos., 119, 4874–4887, doi:10.1002/2013JD020918, 2014.

Karion, A., Sweeney, C., Pétron, G., Frost, G., Hardesty, R. M., Kofler, J., Miller, B. R., Newberger, T., Wolter, S., Banta, R., Brewer, A., Dlugokencky, E., Lang, P., Montzka, S. A., Schnell, R., Tans, P., Trainer, M., Zamora, R., and Conley, S.: Methane emissions estimate from airborne measurements over a western United States natural gas field, Geophys. Res. Lett., 40, 4393–4397, doi:10.1002/grl.50811, 2013.

Kirschke, S., Bousquet, P., Ciais, P., Saunois, M., Canadell, J. G., Dlugokencky, E. J., Bergamaschi, P., Bergmann, D., Blake, D. R., Bruhwiler, L., Cameron-Smith, P., Castaldi, S., Chevallier, F., Feng, L., Fraser, A., Heimann, M., Hodson, E. L., Houweling, S., Josse, B., Fraser, P. J., Krummel, P. B., Lamarque, J.-F., Langenfelds, R. L., Le Quéré, C., Naik, V., O'Doherty, S., Palmer, P. I., Pison, I., Plummer, D., Poulter, B., Prinn, R. G., Rigby, M., Ringeval, B., Santini, M., Schmidt, M., Shindell, D. T., Simpson, I. J., Spahni, R., Steele, L. P., Strode, S. A., Sudo, K., Szopa, S., van der Werf, G. R., Voulgarakis, A., van Weele, M., Weiss, R. F., Williams, J. E., and Zeng, G.: Three decades of global methane sources and sinks, Nat. Geosci., 6, 813–823, doi:10.1038/ngeo1955, 2013.

Kort, E. A., Eluszkiewicz, J., Stephens, B. B., Miller, J. B., Gerbig, C., Nehrkorn, T., Daube, B. C., Kaplan, J. O., Houweling, S., and Wofsy, S. C.: Emissions of CH_4 and N_2O over the United States and Canada based on a receptor-oriented modeling framework and COBRA-NA atmospheric observations, Geophys. Res. Lett., 35, 1–5, doi:10.1029/2008GL034031, 2008.

Kort, E. A., Wofsy, S. C., Daube, B. C., Diao, M., Elkins, J. W., Gao, R. S., Hintsa, E. J., Hurst, D. F., Jimenez, R., Moore, F. L., Spackman, J. R., and Zondlo, M. A.: Atmospheric observations of Arctic Ocean methane emissions up to 82° north, Nat. Geosci., 5, 318–321, doi:10.1038/ngeo1452, 2012.

Krinner, G., Viovy, N., de Noblet-Ducoudré, N., Ogée, J., Polcher, J., Friedlingstein, P., Ciais, P., Sitch, S., and Prentice, I. C.: A dynamic global vegetation model for studies of the coupled atmosphere–biosphere system, Global Biogeochem. Cy., 19, 1–33, doi:10.1029/2003GB002199, 2005.

AMTD
8, 8859–8902, 2015

McManus, J. B., Kebabian, P. L., and Zahniser, M. S.: Astigmatic mirror multi-pass absorption cells for long-path-length spectroscopy, Appl. Optics, 34, 3336–3348, doi:10.1364/AO.34.003336, 1995.

Miller, S. M., Wofsy, S. C., Michalak, A. M., Kort, E. A., Andrews, A. E., Biraud, S. C., Dlugokencky, E. J., Eluszkiewicz, J., Fischer, M. L., Janssens-Maenhout, G., Miller, B. R., Miller, J. B., Montzka, S. A., Nehrkorn, T., and Sweeney, C.: Anthropogenic emissions of methane in the United States., P. Natl. Acad. Sci. USA, 110, 20018–20022, doi:10.1073/pnas.1314392110, 2013.

Myhre, G., Shindell, D., Bréon, F.-M., Collins, W., Fuglestvedt, J., Huang, J., Koch, D., Lamarque, J.-F., Lee, D., Mendoza, B., Nakajima, T., Robock, A., Stephens, G., Takemura, T., and Zhang, H.: Anthropogenic and natural radiative forcing, in: Climate Change 2013: The Physical Science Basis. Contribution of Working Group I to the Fifth Assessment Report of the Intergovernmental Panel on Climate Change, edited by: Stocker, T. F., Qin, D., Plattner, G.-K., Tignor, M., Allen, S. K., Boschung, J., Nauels, A., Xia, Y., Bex, V., and Midgley, P. M., Cambridge University Press, Cambridge, United Kingdom and New York, NY, USA, 659–740, 2013.

Nelson, D. D., Shorter, J. H., McManus, J. B., and Zahniser, M. S.: Sub-part-per-billion detection of nitric oxide in air using a thermoelectrically cooled mid-infrared quantum cascade laser spectrometer, Appl. Phys. B-Lasers O., 75, 343–350, doi:10.1007/s00340-002-0979-4, 2002.

Nelson, D. D., McManus, B., Urbanski, S., Herndon, S., and Zahniser, M. S.: High precision measurements of atmospheric nitrous oxide and methane using thermoelectrically cooled mid-infrared quantum cascade lasers and detectors., Spectrochim. Acta A, 60, 3325–3335, doi:10.1016/j.saa.2004.01.033, 2004.

O'Shea, S. J., Allen, G., Gallagher, M. W., Bauguitte, S. J.-B., Illingworth, S. M., Le Breton, M., Muller, J. B. A., Percival, C. J., Archibald, A. T., Oram, D. E., Parrington, M., Palmer, P. I., and Lewis, A. C.: Airborne observations of trace gases over boreal Canada during BORTAS: campaign climatology, air mass analysis and enhancement ratios, Atmos. Chem. Phys., 13, 12451–12467, doi:10.5194/acp-13-12451-2013, 2013a.

O'Shea, S. J., Bauguitte, S. J.-B., Gallagher, M. W., Lowry, D., and Percival, C. J.: Development of a cavity-enhanced absorption spectrometer for airborne measurements of CH_4 and CO_2, Atmos. Meas. Tech., 6, 1095–1109, doi:10.5194/amt-6-1095-2013, 2013b.

AMTD
8, 8859–8902, 2015

O'Shea, S. J., Allen, G., Fleming, Z. L., Bauguitte, S. J.-B., Percival, C. J., Gallagher, M. W., Lee, J., Helfter, C., and Nemitz, E.: Area fluxes of carbon dioxide, methane, and carbon monoxide derived from airborne measurements around Greater London: a case study during summer 2012, J. Geophys. Res.-Atmos., 119, 4940–4952, doi:10.1002/2013JD021269, 2014a.

O'Shea, S. J., Allen, G., Gallagher, M. W., Bower, K., Illingworth, S. M., Muller, J. B. A., Jones, B. T., Percival, C. J., Bauguitte, S. J-B., Cain, M., Warwick, N., Quiquet, A., Skiba, U., Drewer, J., Dinsmore, K., Nisbet, E. G., Lowry, D., Fisher, R. E., France, J. L., Aurela, M., Lohila, A., Hayman, G., George, C., Clark, D. B., Manning, A. J., Friend, A. D., and Pyle, J.: Methane and carbon dioxide fluxes and their regional scalability for the European Arctic wetlands during the MAMM project in summer 2012, Atmos. Chem. Phys., 14, 13159–13174, doi:10.5194/acp-14-13159-2014, 2014b.

Peischl, J., Ryerson, T. B., Holloway, J. S., Parrish, D. D., Trainer, M., Frost, G. J., Aikin, K. C., Brown, S. S., Dubé, W. P., Stark, H., and Fehsenfeld, F. C.: A top-down analysis of emissions from selected Texas power plants during TexAQS 2000 and 2006, J. Geophys. Res., 115, D16303, doi:10.1029/2009JD013527, 2010.

Peischl, J., Ryerson, T. B., Aikin, K. C., Gouw, J. A., Gilman, J. B., Holloway, J. S., Lerner, B. M., Nadkarni, R., Neuman, J. A., Nowak, J. B., Trainer, M., Warneke, C., and Parrish, D. D.: Quantifying atmospheric methane emissions from the Haynesville, Fayetteville, and northeastern Marcellus shale gas production regions, J. Geophys. Res.-Atmos., 120, 2119–2139, doi:10.1002/2014JD022697, 2015.

Polson, D., Fowler, D., Nemitz, E., Skiba, U., McDonald, A., Famulari, D., Di Marco, C., Simmons, I., Weston, K., and Purvis, R.: Estimation of spatial apportionment of greenhouse gas emissions for the UK using boundary layer measurements and inverse modelling technique, Atmos. Environ., 45, 1042–1049, doi:10.1016/j.atmosenv.2010.10.011, 2011.

Rannik, Ü., Haapanala, S., Shurpali, N. J., Mammarella, I., Lind, S., Hyvönen, N., Peltola, O., Zahniser, M., Martikainen, P. J., and Vesala, T.: Intercomparison of fast response commercial gas analysers for nitrous oxide flux measurements under field conditions, Biogeosciences, 12, 415–432, doi:10.5194/bg-12-415-2015, 2015.

Ravishankara, A. R., Daniel, J. S., and Portmann, R. W.: Nitrous oxide (N_2O): the dominant ozone-depleting substance emitted in the 21st century, Science, 123, 123–125, doi:10.1126/science.1176985, 2007.

AMTD
8, 8859–8902, 2015

Rella, C. W., Chen, H., Andrews, A. E., Filges, A., Gerbig, C., Hatakka, J., Karion, A., Miles, N. L., Richardson, S. J., Steinbacher, M., Sweeney, C., Wastine, B., and Zellweger, C.: High accuracy measurements of dry mole fractions of carbon dioxide and methane in humid air, Atmos. Meas. Tech., 6, 837–860, doi:10.5194/amt-6-837-2013, 2013.

Ritter, J. A., Barrick, J. D. W., Sachse, G. W., Gregory, G. L., Woerner, M. A., Watson, C. E., Hill, G. F., and Collins, J. E.: Airborne flux measurements of trace species in an Arctic boundary layer, J. Geophys. Res., 97, 16601–16625, doi:10.1029/92JD01812, 1992.

Rothman, L. S., Gordon, I. E., Babikov, Y., Barbe, A., Chris Benner, D., Bernath, P. F., Birk, M., Bizzocchi, L., Boudon, V., Brown, L. R., Campargue, A., Chance, K., Cohen, E. A., Coudert, L. H., Devi, V. M., Drouin, B. J., Fayt, A., Flaud, J.-M., Gamache, R. R., Harrison, J. J., Hartmann, J.-M., Hill, C., Hodges, J. T., Jacquemart, D., Jolly, A., Lamouroux, J., Le Roy, R. J., Li, G., Long, D. A., Lyulin, O. M., Mackie, C. J., Massie, S. T., Mikhailenko, S., Müller, H. S. P., Naumenko, O. V., Nikitin, A. V., Orphal, J., Perevalov, V., Perrin, A., Polovtseva, E. R., Richard, C., Smith, M. A. H., Starikova, E., Sung, K., Tashkun, S., Tennyson, J., Toon, G. C., Tyuterev, V. G., and Wagner, G.: The HITRAN2012 molecular spectroscopic database, J. Quant. Spectrosc. Ra., 130, 4–50, doi:10.1016/j.jqsrt.2013.07.002, 2013.

Santoni, G. W., Daube, B. C., Kort, E. A., Jiménez, R., Park, S., Pittman, J. V., Gottlieb, E., Xiang, B., Zahniser, M. S., Nelson, D. D., McManus, J. B., Peischl, J., Ryerson, T. B., Holloway, J. S., Andrews, A. E., Sweeney, C., Hall, B., Hintsa, E. J., Moore, F. L., Elkins, J. W., Hurst, D. F., Stephens, B. B., Bent, J., and Wofsy, S. C.: Evaluation of the airborne quantum cascade laser spectrometer (QCLS) measurements of the carbon and greenhouse gas suite – CO_2, CH_4, N_2O, and CO – during the CalNex and HIPPO campaigns, Atmos. Meas. Tech., 7, 1509–1526, doi:10.5194/amt-7-1509-2014, 2014.

Syakila, A. and Kroeze, C.: The global nitrous oxide budget revisited, Greenhouse Gas Measurement and Management, 1, 17–26, doi:10.3763/ghgmm.2010.0007, 2011.

Tanaka, T., Miyamoto, Y., Morino, I., Machida, T., Nagahama, T., Sawa, Y., Matsueda, H., Wunch, D., Kawakami, S., and Uchino, O.: Aircraft measurements of carbon dioxide and methane for the calibration of ground-based high-resolution Fourier Transform Spectrometers and a comparison to GOSAT data measured over Tsukuba and Moshiri, Atmos. Meas. Tech., 5, 2003–2012, doi:10.5194/amt-5-2003-2012, 2012.

Thompson, R. L., Ishijima, K., Saikawa, E., Corazza, M., Karstens, U., Patra, P. K., Bergamaschi, P., Chevallier, F., Dlugokencky, E., Prinn, R. G., Weiss, R. F., O'Doherty, S., Fraser, P. J., Steele, L. P., Krummel, P. B., Vermeulen, A., Tohjima, Y., Jordan, A., Haszpra, L.,

AMTD
8, 8859–8902, 2015

Steinbacher, M., Van der Laan, S., Aalto, T., Meinhardt, F., Popa, M. E., Moncrieff, J., and Bousquet, P.: TransCom N_2O model inter-comparison – Part 2: Atmospheric inversion estimates of N_2O emissions, Atmos. Chem. Phys., 14, 6177–6194, doi:10.5194/acp-14-6177-2014, 2014.

Webb, N., Broomfield, M., Brown, P., Buys, G., Cardenas, L., Murrells, T., Pang, Y., Passant, N., Thistlethwaite, G., and Watterson, J.: UK Greenhouse Gas Inventory 1990 to 2012: annual report for submission under the framework convention on climate change, Department of Energy and Climate Change, Harwell, Didcot, Oxfordshire, 2014.

Wecht, K. J., Jacob, D. J., Wofsy, S. C., Kort, E. A., Worden, J. R., Kulawik, S. S., Henze, D. K., Kopacz, M., and Payne, V. H.: Validation of TES methane with HIPPO aircraft observations: implications for inverse modeling of methane sources, Atmos. Chem. Phys., 12, 1823–1832, doi:10.5194/acp-12-1823-2012, 2012.

Werle, P., Mücke, R., and Slemr, F.: The limits of signal averaging in atmospheric trace-gas monitoring by tunable diode-laser absorption spectroscopy (TDLAS), Appl. Phys. B-Photo., 57, 131–139, doi:10.1007/BF00425997, 1993.

WMO: GAW Report No. 185 Guidelines for the Measurement of Methane and Nitrous Oxide and their Quality Assurance, World Meteorological Organization, Geneva, Switzerland, 2009.

WMO: GAW Report No. 213, 17th WMO/IAEA Meeting on Carbon Dioxide, Other Greenhouse Gases and Related Tracers Measurement Techniques (GGMT-2013), World Meteorological Organization, Geneva, Switzerland, 2013.

Wofsy, S. C., the HIPPO Science Team and Cooperating Modellers and Satellite Teams: HIAPER Pole-to-Pole Observations (HIPPO): fine-grained, global-scale measurements of climatically important atmospheric gases and aerosols., Philos. T. R. Soc. A, 369, 2073–2086, doi:10.1098/rsta.2010.0313, 2011.

Xiang, B., Miller, S. M., Kort, E. A., Santoni, G. W., Daube, B. C., Commane, R., Angevine, W. M., Ryerson, T. B., Trainer, M. K., Andrews, A. E., Nehrkorn, T., Tian, H., and Wofsy, S. C.: Nitrous oxide (N_2O) emissions from California based on 2010 CalNex airborne measurements, J. Geophys. Res.-Atmos., 118, 2809–2820, doi:10.1002/jgrd.50189, 2013.

Yuan, B., Kaser, L., Karl, T., Graus, M., Peischl, J., Campos, T. L., Shertz, S., Apel, E. C., Hornbrook, R. S., Hills, A., Gilman, J. B., Lerner, B. M., Warneke, C., Flocke, F. M., Ryerson, T. B., Guenther, A. B., and de Gouw, J. A.: Airborne flux measurements of methane and

AMTD
8, 8859–8902, 2015

volatile organic compounds (VOCs) over the Haynesville and Marcellus shale gas production regions, J. Geophys. Res.-Atmos., 120, 6271–6289, doi:10.1002/2015JD023242, 2015.

Zahniser, M. S., Nelson, D. D., McManus, J. B., Kebabian, P. L., and Lloyd, D.: Measurement of trace gas fluxes using tunable diode laser spectroscopy, Philosophical Transactions: Physical Sciences and Engineering, 351, 371–382, 1995.

Zellweger, C., Steinbacher, M., and Buchmann, B.: Evaluation of new laser spectrometer techniques for in-situ carbon monoxide measurements, Atmos. Meas. Tech., 5, 2555–2567, doi:10.5194/amt-5-2555-2012, 2012.

Zhuang, Q., Melillo, J. M., Sarofim, M. C., Kicklighter, D. W., McGuire, A. D., Felzer, B. S., Sokolov, A., Prinn, R. G., Steudler, P. A., and Hu, S.: CO_2 and CH_4 exchanges between land ecosystems and the atmosphere in northern high latitudes over the 21st century, Geophys. Res. Lett., 33, 2–6, doi:10.1029/2006GL026972, 2006.

AMTD
8, 8859–8902, 2015

Table 1. Mean and standard deviation of the difference between QCLAS 1 Hz target cylinder measurements and the nominal cylinder values, and the difference between the 1 Hz QCLAS and the corresponding 1 Hz FGGA sample CH_4 measurements, using both the original and pressure-differentiated calibration methods.

	QCLAS-target difference (ppb)				QCLAS-FGGA difference (ppb)	
	N_2O		CH_4		CH_4	
Calibration Method	Mean	1σ	Mean	1σ	Mean	1σ
Original	0.00319	0.960	0.253	4.78	−2.87	8.27
Pressure-differentiated	0.105	0.419	0.0668	1.71	−2.05	5.85

AMTD
8, 8859–8902, 2015

Table 2. The fraction of 1 Hz data within the WMO compatibility recommendations for QCLAS target cylinder measurement and QCLAS/FGGA sample measurement, using both the original and pressure-differentiated calibration methods.

	QCLAS-target		QCLAS-FGGA
Calibration Method	N_2O	CH_4	CH_4
Original	0.149	0.519	0.292
Pressure-differentiated	0.309	0.765	0.361

AMTD
8, 8859–8902, 2015

Table 3. Allan Precision for QCLAS measurement of CH_4 and N_2O, both during ambient in-flight sampling and whilst sampling a compressed air cylinder in the laboratory, given for averaging times of 1, 10 and 108 s.

	1σ Allan Precision (ppb)					
	1 s		10 s		108 s	
	Flight	Lab	Flight	Lab	Flight	Lab
CH_4	0.52	0.48	0.31	0.17	0.23	0.12
N_2O	0.11	0.12	0.074	0.044	0.042	0.029

AMTD
8, 8859–8902, 2015

Table 4. Known component and nominal total uncertainties for the QCLAS measurement of CH_4 and N_2O, calibrated using the pressure-differentiated method.

	1σ Uncertainty (ppb)			
	Water vapour correction	Target standard calibration	In-flight target measurements	Total
CH_4	1.63	0.77	0.07	1.81
N_2O	0.32	0.11	0.10	0.35

AMTD
8, 8859–8902, 2015

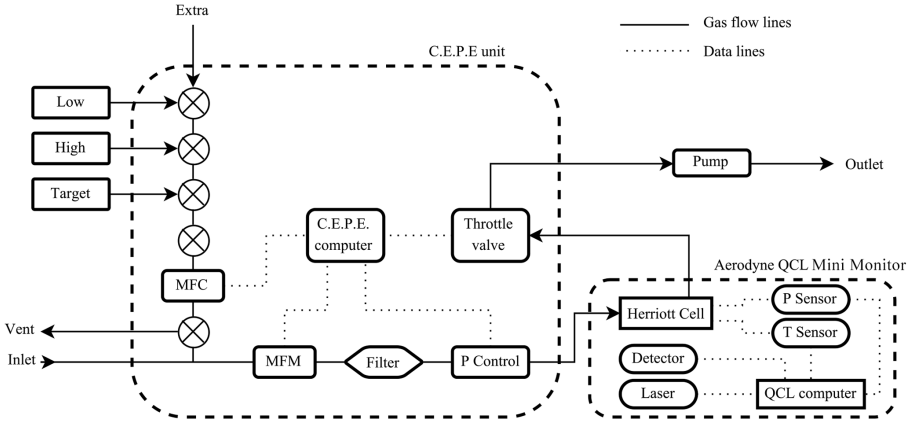

Figure 1. Schematic showing the QCLAS air sampling and data handling systems. The C.E.P.E. (Calibration, Exhaust, Power and Electronics) unit and the Aerodyne QCL Mini Monitor enclosures are represented by dashed boxes around the components they contain. The calibration cylinders are labelled "Low", "High", and "Target". The flow rate of the calibration gas is controlled by the MFC (mass flow controller), and the flow rate into the instrument is monitored by the MFM (mass flow meter). The optical components associated with the alignment of the laser beam are not shown.

AMTD
8, 8859–8902, 2015

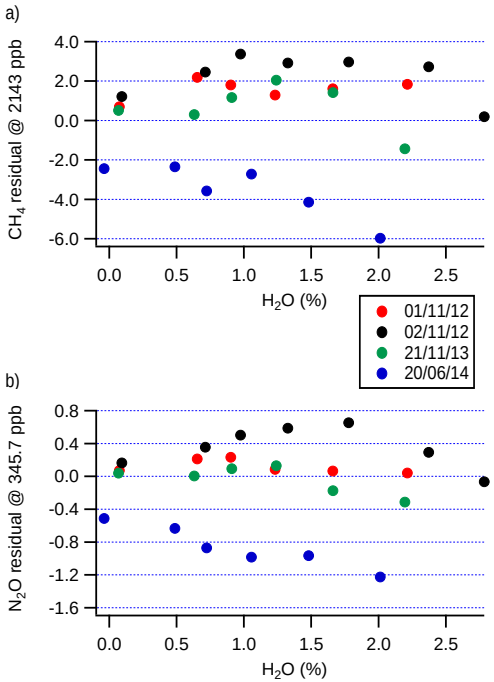

Figure 2. Residual error due to the influence of water vapour for the retrieval of **(a)** CH_4 and **(b)** N_2O after applying an empirically derived scale factor to correct the data. Data from four identical experiments is shown; the residuals are calculated as the product of the fractional error for each measurement and the average mole fraction for the dry measurements taken during all four experiments.

AMTD
8, 8859–8902, 2015

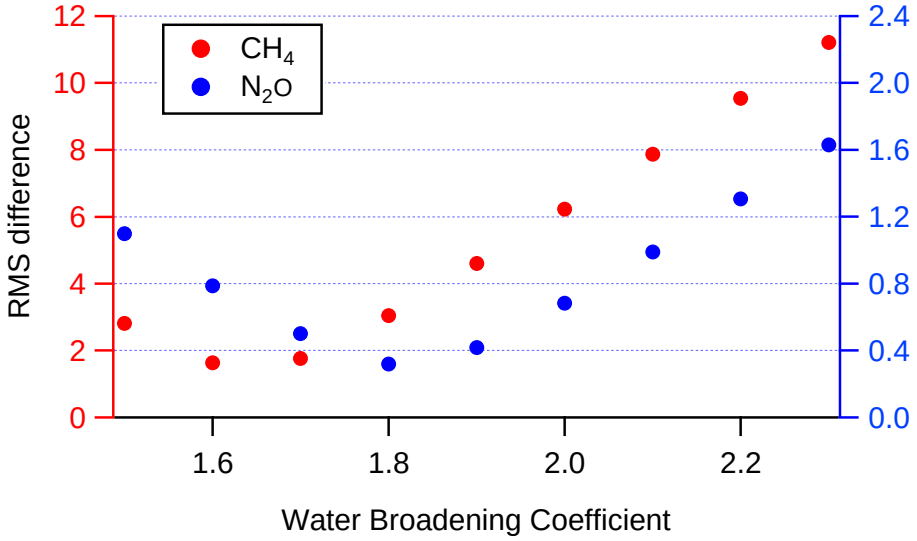

Figure 3. RMS (root mean square) difference between the retrieved wet mole fractions and the corresponding dry measurements for CH_4 and N_2O, as a function of water broadening coefficient. These RMS values are determined using data taken over the full experimental range of H_2O mole fraction during all four identical experiments.

AMTD
8, 8859–8902, 2015

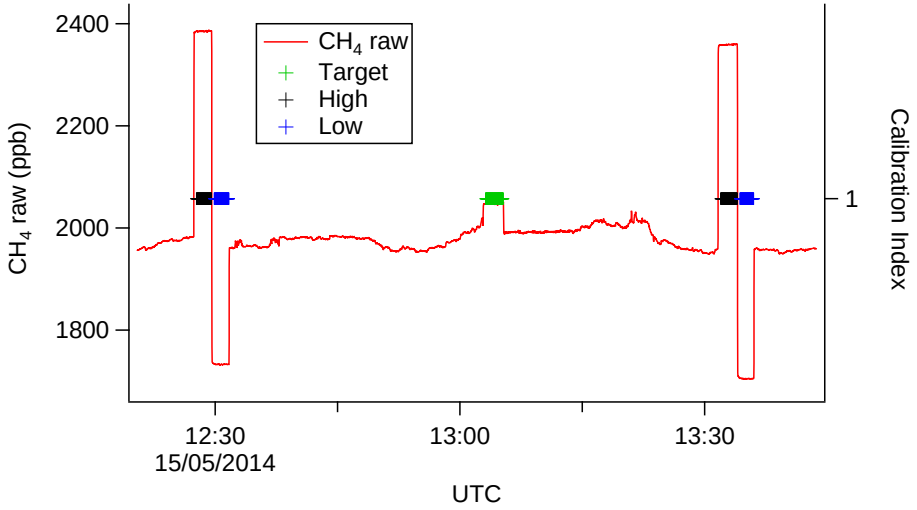

Figure 4. A selection of raw CH_4 data from flight B848, overlaid with calibration index markers to highlight the hourly calibration cycle. The target cylinder measurement (green markers) is performed approximately mid-way between the high-low span cylinder measurements (black and blue markers respectively) used to calibrate the data to the WMO scale.

AMTD
8, 8859–8902, 2015

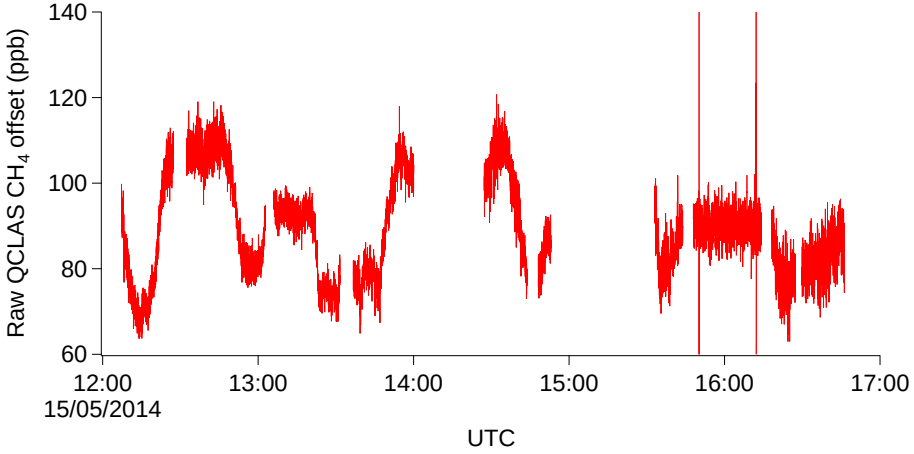

Figure 5. The offset between the raw QCLAS CH_4 data and the calibrated FGGA data (used here as our reference) during flight B848. Gradients of over 30 ppb in less than 10 min can be seen to be present.

AMTD
8, 8859–8902, 2015

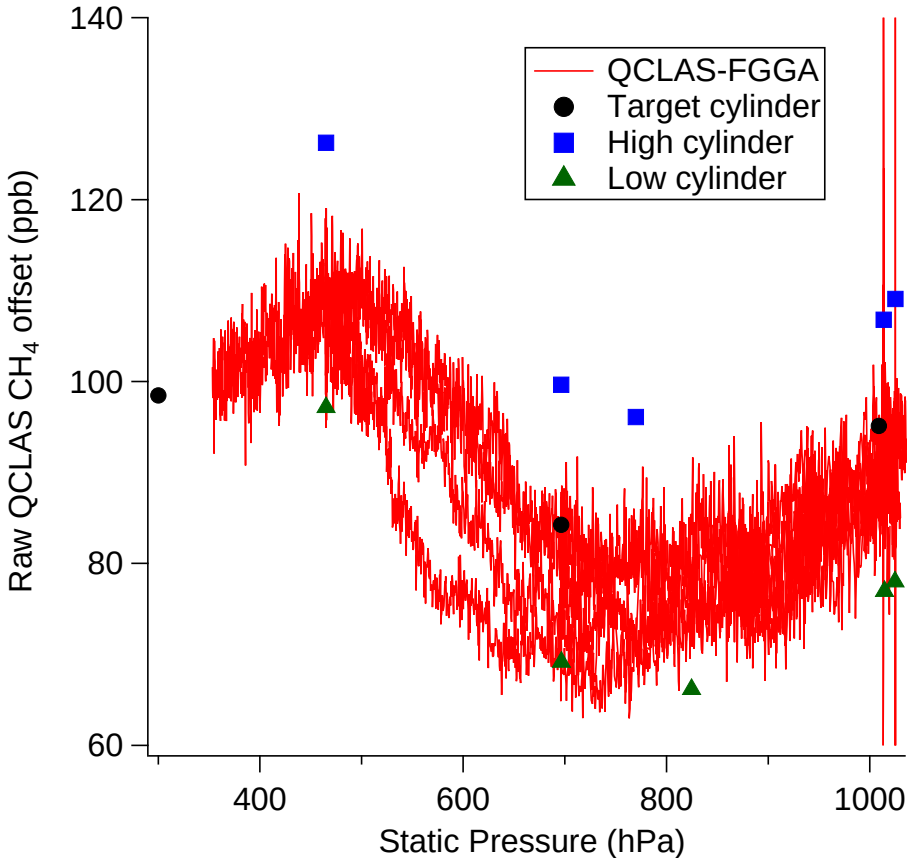

Figure 6. The offset between the raw QCLAS CH_4 measurements and both the corresponding calibrated FGGA data and the known contents of the target, high and low calibration cylinders during flight B848, shown as a function of static pressure. Although the absolute magnitude of the offset differs for these four different measurements, the same broadly repeatable pattern is exhibited by each of them.

AMTD
8, 8859–8902, 2015

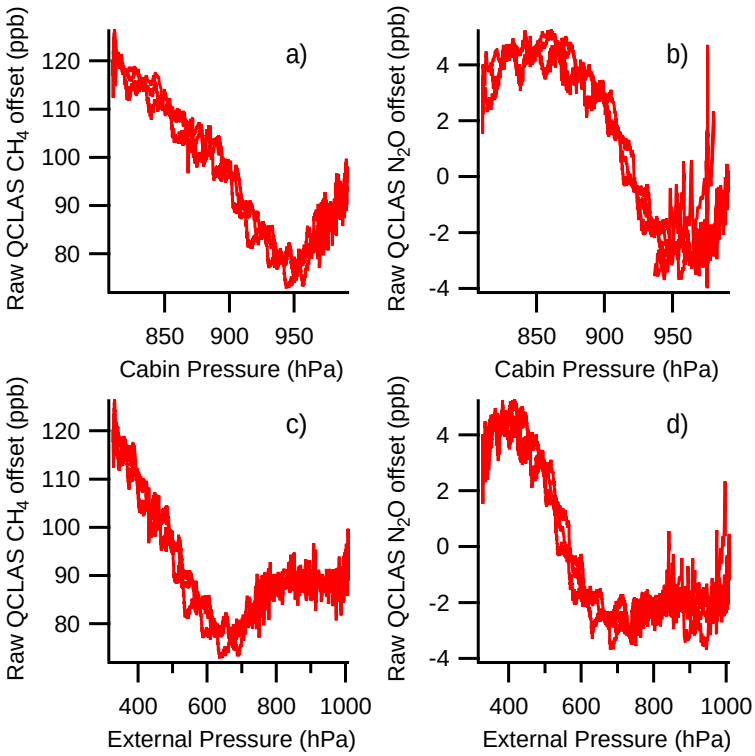

Figure 7. The offset between the raw retrieved QCLAS mole fractions and the known content of a target cylinder, sampled continuously during three separate deep profiles. Panels (**a**) and (**b**) show the offset as a function of the pressure inside the cabin for CH_4 and N_2O respectively. Panels (**c**) and (**d**) show the offset as a function of external static pressure (also for CH_4 and N_2O respectively).

AMTD
8, 8859–8902, 2015

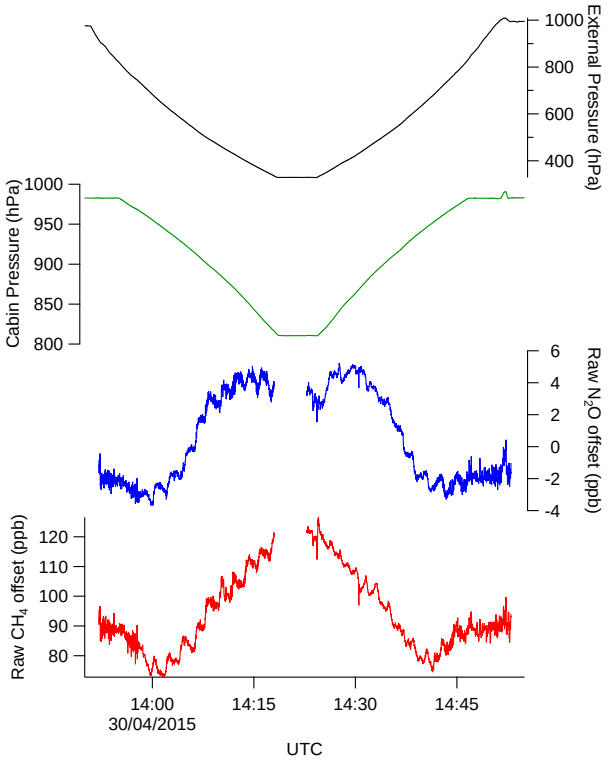

Figure 8. Time series showing the offset between the raw retrieved QCLAS mole fractions and the known content of the target cylinder being sampled. Cabin pressure and external static pressure are also shown to illustrate the systematic nature of the offset during two consecutive profiles.

AMTD
8, 8859–8902, 2015

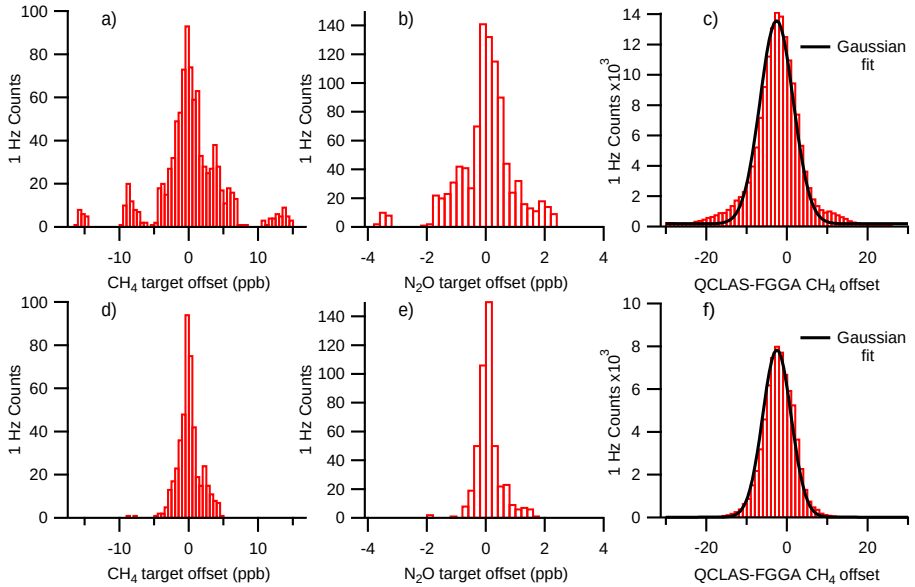

Figure 9. Histograms showing the offset between the calibrated 1 Hz QCLAS measurements and both the corresponding target cylinder values and the corresponding FGGA sample measurements. Panels **(a)**–**(c)** show histograms for data calibrated using the original method; in comparison panels **(d)**–**(f)** show the corresponding histograms using the pressure-differentiated calibration method. It can be seen here that the pressure-differentiated method results in the removal of many of the outlying target cylinder measurements. In addition, the Gaussian fit to the QCLAS-FGGA CH_4 offset is also improved by the pressure-differentiated calibration method (panel **f**) relative to the original method (panel **c**).

AMTD
8, 8859–8902, 2015

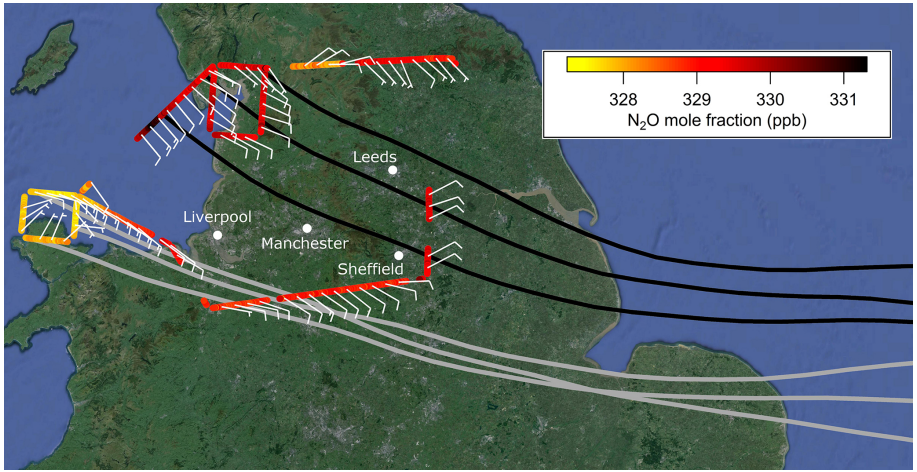

Figure 10. Aircraft flight track for flight B868, coloured by N_2O mole fraction. Average wind speeds and directions taken over 60 s are shown as a wind barbs (using the convention where each full barb represents a wind speed of 10 knots). Selected HYSPLIT back trajectories are shown for a region of enhanced N_2O (black) and a contrasting region of lower N_2O (grey). Map data: Google, SIO, NOAA, U.S. Navy, NGA, GEBCO, Landsat.

AMTD
8, 8859–8902, 2015